Oguzer et al. Journal of the European Optical Society-Rapid Publications (2017) 13:16
DOI 10.1186/s41476-017-0041-0

Journal of the European Optical Society-Rapid Publications

RESEARCH Open Access

Focusing of THz waves with a microsize parabolic reflector made of graphene in the free space

Taner Oguzer[1], Ayhan Altintas[2] and Alexander I. Nosich[3*]

Abstract

Background: The scattering of H- and E-polarized plane waves by a two-dimensional (2-D) parabolic reflector made of graphene and placed in the free space is studied numerically.

Methods: To obtain accurate results we use the Method of Analytical Regularization.

Results: The total scattering cross-section and the absorption cross-section are computed, together with the field magnitude in the geometrical focus of reflector. The surface plasmon resonances are observed in the H-case. The focusing ability of the reflector is studied in dependence of graphene's chemical potential, frequency, and reflector's depth.

Conclusions: It is found that there exists an optimal range of frequencies where the focusing ability reaches maximum values. The reason is the quick degradation of graphene's surface conductivity with frequency.

Keywords: Graphene reflector, Focusing ability, Integral equation, Analytical regularization

Background

Graphene, which is a monolayer (1 nm) or a very thin (2-3 nm) stack of a few layers of graphite ([1–3], see Fig. 1-c in [3]), is a non-conventional material famous for being electrically conductive, mechanically strong and optically transparent. Due to the inductive nature of the associated complex-valued surface impedance, it can support the Surface Plasmon (SP) wave [1]. This wave can be strongly reflected back from the edges of patterned graphene so that natural SP modes (standing waves) can occur, in the Fabry-Perot type manner. This phenomenon has been observed at the frequencies varying from the infrared for the nano-size flat graphene samples [3] to the THz range for the micro-size ones [2]. It is already exploited in the nanosensor devices [3, 4].

Important feature of graphene is that its conductivity can be controlled by applying an external electrostatic biasing field which modifies graphene's chemical potential. Usually this requires a dielectric substrate although suspended graphene is also realizable [5]. Therefore in the modeling, one can consider a curved graphene strip located in the free space, and assume that the d-c bias is still present. Note also that the edge effects become important only if a graphene strip width is smaller than 100 nm. For wider strips one can disregard the edge effects and use the electron conductivity model developed for infinite graphene layer. In the THz range this requirement is well satisfied for micro-size strips.

One of the interesting questions in this area is how well the THz wave can be focused with a curved reflector made of graphene. The goal of this paper is to answer this question for a 2-D parabolic reflector as depicted in Fig. 1. We perform such a study using the electromagnetic boundary value problem (BVP), which includes the resistive-sheet boundary condition originally derived for thinner-than-skindepth imperfect (partially transparent) metal layers [6, 7].

We consider both the H- and the E-polarization cases where electric field is in the plane of reflector's cross-section and in parallel to reflector, respectively. It should be noted that, similarly to the full-wave modeling of perfectly electrically conducting (PEC) reflectors, finite-difference time-domain method can be considered as one of possible computational instruments. However it leads to huge number of unknowns due to the discretization of large physical domain and also has a disadvantage in the

* Correspondence: anosich@yahoo.com
[3]Laboratory of Micro and Nano Optics, Institute of Radio-Physics and Electronics NASU, Kharkiv 61085, Ukraine
Full list of author information is available at the end of the article

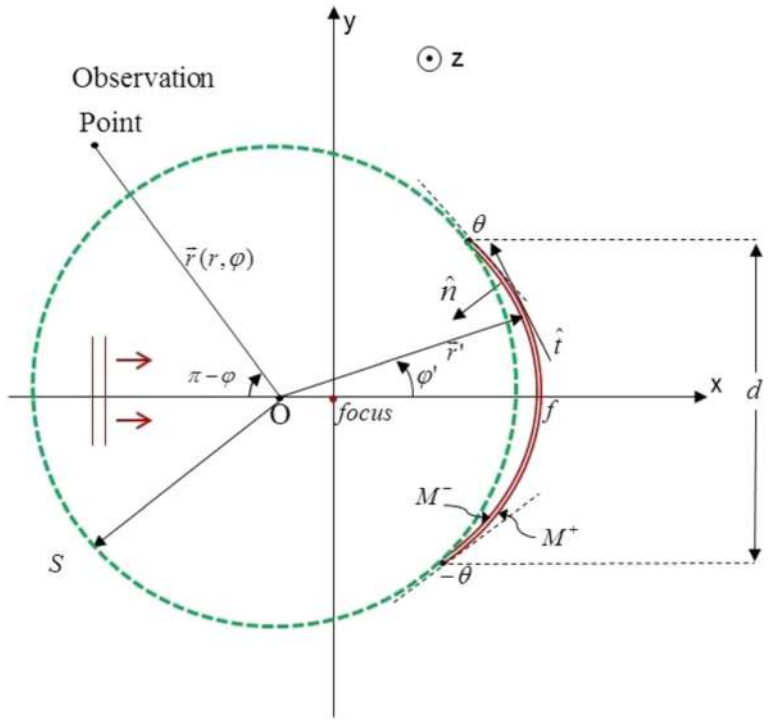

Fig. 1 Cross-sectional geometry of a parabolic graphene reflector in the free space, illuminated with a plane wave

inability to satisfy the far field radiation condition. The method of moments (MoM) procedure can be also applied to treat singular integral equations (SIE) derived for arbitrary reflectors. However conventional MoM with local basis and testing functions has overall accuracy at the level of 2-3 digits even when treating the medium size reflectors (10 wavelengths). If better accuracy is needed or larger reflectors are interested in, one hits non-realistic computation times or complete failure of the code because of the quick growth of the matrix condition number. Another alternative is the high frequency techniques like geometrical and physical optics, which work much faster however do not produce accurate full-wave results.

All mentioned above is especially important in the case of H-polarization where the associated SIE has hyper-type singularity. Attractive way out of that pitfall is offered by the method of analytical regularization (MAR) [8]. With MAR, the kernel of the associated SIE for the current on the reflector is presented as a sum of two parts, a more singular part (usually static) and a remainder. Then the more singular part is analytically inverted by using some special technique like the Riemann-Hilbert Problem (RHP) method [7, 9, 10]. The remainder leads to the Fredholm second-kind matrix equation that provides a convergent numerical solution. The same can be achieved by choosing the global expansion functions that are orthogonal eigenfunctions of the hyper-singular part of SIE operator and using them in a MoM-like Galerkin projection algorithm [11]. In either case the SIE-MAR technique enables accurate and economic full-wave analysis of electromagnetic scattering problems for both PEC and imperfect reflectors. For instance, in [9], the H-wave scattering and the focusing were studied for the resistive 2-D reflectors having elliptical contours.

In the E-polarization case, the associated SIE has a logarithmically singular kernel [12] and hence is already a Fredholm second kind equation. This guarantees convergence of discretization schemes. Still projecting it on the set of entire-domain expansion functions brings additional advantages and makes the resulting numerical algorithm more economic. The E-polarized beam scattering and collimation by parabolic resistive reflectors was analyzed in this manner in [12].

Note that the scattering and absorption of THz waves by a single flat graphene strip and finite graphene-strip gratings was reduced to SIE and its Nystrom type solution was built in [13, 14]. Infinite graphene-strip grating in the free space was also studied by the MAR-RHP technique in [10]. In these works, the field characteristics were investigated as a function of graphene and grating parameters showing the presence of SP resonances. In more recent works [4, 15], the bulk refractive index sensitivities of the THz range SP resonances were studied for a micro-size graphene strip and a dielectric tube covered with graphene, respectively.

Following the mentioned and other works, we simulate graphene with the aid of the resistive-sheet boundary condition together with the Kubo formula for the graphene

electron conductivity. We derive a corresponding SIE from the electromagnetic BVP and solve it using the RHP-based MAR solution. This type of algorithm provides us accurate data for the quantifications of the scattering, absorption and focusing characteristics. As a result, we obtain the frequency scans of the total scattering and absorption cross sections (TSCS and ACS) of a 2-D parabolic graphene reflector and in the H-case identify the SP resonances. Then we perform a study of the focusing ability of such a curved strip as a 2-D reflector for various graphene parameters.

Preliminary results of such analysis were reported at a conference [16]; here we present new and more complete numerical study and obtain better insight into the studied effects.

Methods

The problem geometry of a 2-D parabolic graphene reflector frontally illuminated by a plane wave is presented in Fig. 1. Reflector's contour M is defined as a finite parabolic profile. An auxiliary closed contour denoted as C is the contour M completed with the circular arc S, which must have the same curvature as the reflector at the latter's edge points. Such a smooth contour C is necessary for obtaining the regularized (i.e. Fredholm second kind) matrix equation - see [9, 12].

The rigorous formulation of the considered BVP involves the Helmholtz equation, the Sommerfeld radiation condition far from the reflector, the resistive boundary condition on M, and an edge condition such that the field power is limited in any finite domain around the reflector edge. Collectively, these conditions guarantee the uniqueness of the problem solution.

The resistive boundary condition on a zero-thickness sheet is a well-established model of a thin penetrable sheet, e.g. a metal thinner than skin depth or a very thin dielectric layer. In view of "atomic" thickness of graphene, the same boundary condition can also be used for a flat or curved graphene surface, avoiding introduction the thickness of graphene of 2-3 nm that generates meshing troubles in the use of purely numerical codes like COMSOL. It can be written as the following two equations valid at $\vec{r}\in M$:

$$\left(\vec{E}^{+}_{\tan}+\vec{E}^{-}_{\tan}\right)/2 = Z\,\vec{n}\times\left(\vec{H}^{+}_{\tan}-\vec{H}^{-}_{\tan}\right),\quad \vec{E}^{+}_{\tan}=\vec{E}^{-}_{\tan}, \tag{1}$$

where the subscript "tan" indicates the tangential field, the superscripts "- " and "+" relate to the front and back faces of reflector, respectively, and $\vec{n}$ is understood as the unit vector normal to the concave side of reflector. The jump in the tangential magnetic field, $\vec{J}=\vec{H}^{+}_{\tan}-\vec{H}^{-}_{\tan}$, is unknown function of the electric surface-current density, and the coefficient Z is graphene's surface impedance [1–5].

Note also that the surface impedance is related to the graphene surface electron conductivity σ as $Z = 1/\sigma$, and the conductivity can be found as the Kubo sum of intraband and interband contributions [1–6]. As condition (1) was derived for infinite planar layer, in the modeling of the wave-scattering by finite surfaces it must be combined with the edge condition to provide the uniqueness of the BVP solution.

In the H-wave case, on using the boundary condition (1) we obtain a hyper-singular SIE for the surface current J_t on the reflector. On integrating by parts, it can be cast to the following form:

$$\begin{aligned} ZJ_t - \frac{iZ_0}{k}\frac{\partial}{\partial l}\int_M\left[\frac{\partial}{\partial l'}J_t\left(\vec{r}'\right)\right]G\left(\vec{r},\vec{r}'\right)dl' \\ +ikZ_0\int_M J_t\left(\vec{r}'\right)\cos\left[\xi\left(\vec{r}\right)-\xi\left(\vec{r}'\right)\right]G\left(\vec{r},\vec{r}'\right)dl' \\ = \frac{iZ_0}{k}\frac{\partial H_z^{in}}{\partial n}, \end{aligned} \tag{2}$$

where the 2-D Green's function G is a Hankel function of zero order and first kind satisfying the radiation condition, i.e. $G\left(\vec{r},\vec{r}'\right) = (i/4)H_{0^{(1)}}(k_oR)$, $R=\left|\vec{r}-\vec{r}'\right|$, and the angle $\xi(\phi)$ is between the normal on M and the x-direction.

Now, we assume that the curve M can be characterized with the aid of the parametric equations $x = x(\phi), y = y(\phi)$, where $0 \le |\phi| \le \theta$, in terms of the polar angle, ϕ. Besides, we denote the differential length in the tangential direction at any point on M as $\partial l = a\beta(\phi)\partial\phi$. We introduce also a function $\beta(\phi) = r(\phi)/[a\cos\gamma(\phi)]$, where $\gamma(\phi)$ is the angle between the normal on M and the radial direction. Then we extend the surface-current density J_t with zero value to arc S and cast IE (2) to a dual equation on the arcs S and M [9].

To continue with the MAR, we add and subtract, from the integral kernels in (2), similar functions at a full circular contour of the same radius as S. The latter operators can be inverted analytically while the remaining ones have smooth kernels,

$$A(\phi,\phi') = H_0^{(1)}(kR) - H_0^{(1)}[2ka\sin(|\phi-\phi'|/2)], \tag{3}$$

$$\begin{aligned} B(\phi,\phi') = {} & \cos[\xi(\phi)-\xi(\phi')]\beta(\phi)\beta(\phi')H_0{}^{(1)}\left[k\left|\vec{r}(\phi)-\vec{r}'(\phi')\right|\right] \\ & -\beta^2(\phi)H_0^{(1)}[2ka\sin(|\phi-\phi'|/2)] \end{aligned} \tag{4}$$

For the inversion of the singular operators, all functions including the incident field should be expanded in terms of the Fourier series in ϕ. Note that the functions

A and B are continuous and have also continuous first derivatives, while their second derivatives with respect to ϕ and ϕ' have only logarithmic singularities and hence belong to L_2. Therefore on the curve C their Fourier coefficients in ϕ decay fast enough with larger indices and hence can be efficiently computed by the Fast Fourier Transform algorithm. Then the discretized version of the SIE and the zero current condition on the aperture S give us a dual series equation. Its semi-inversion, based on the MAR approach using the RHP technique [7, 10], finally produces an algebraic equation set [9]. This infinite matrix equation is of the Fredholm second kind hence the Fredholm theorems guarantee the existence of the unique solution and also the convergence of the approximate numerical solutions when truncating the set with progressively larger orders.

In the E-wave case, on using the boundary condition (1) we obtain the following log-singular IE for the surface current J_z on the reflector:

$$ZJ_z - ikZ_0 \int_M J_z\left(\overrightarrow{r'}\right) G\left(\overrightarrow{r}, \overrightarrow{r'}\right) dl' = E_z^{in}, \tag{5}$$

As mentioned, convergence of usual discretizations of this equation is guaranteed by its Fredholm second-kind nature. Therefore we apply the projection to the set of entire-domain angular exponents [12]. In either polarization case we adapt the matrix truncation number to provide the 4-digit or better accuracy of computations.

The scattered electromagnetic field in the far zone of reflector is a cylindrical wave with functions $H_{z^{sc}}$ or $E_{z^{sc}}$ (depending on the polarization) reduced to $(2/i\pi kr)^{1/2}\, e^{ikr}\, \phi(\phi)$, where $\phi(\phi)$ is the angular scattering pattern. Then TSCS can be obtained by using the following expression:

$$\sigma_{tsc} = \frac{2}{\pi k} \int_0^{2\pi} |\phi(\phi)|^2 d\phi, \tag{6}$$

and ACS of a lossy graphene reflector can be found from the optical theorem,

$$\sigma_{abs} = -\frac{4}{k} \mathrm{Re}\, \phi(0) - \sigma_{tsc} \tag{7}$$

Results and discussion

The numerical accuracy and convergence of the explained above in-house algorithms have already been verified in [9, 12]. In the current work, we apply it to the analysis of both the plane-wave scattering and absorption and the effect of focusing by the graphene reflector.

Therefore, besides of TSCS and ACS defined above, we also calculate another parameter, which serves as a simple figure of merit of the focusing ability (FA), in the plane-wave focusing by a parabolic graphene reflector. In view of the unite-amplitude plane wave incidence, FA can be reasonably defined as the total field magnitude at the geometrical-focus point of parabola.

In Fig. 2, the values of ACS and TSCS are plotted as a function of frequency for two graphene reflectors with the fixed size of $d = 200$ μm (small-size reflector) and $d = 1000$ μm (medium-size reflector), respectively, the both having the same fixed focal ratio f/d.

The oscillations observed on the plots are due to the SP resonances, especially well visible in ACS behavior. Note also that the absorption is by an order of magnitude smaller than the scattering, and the both drop with frequency because of the growth of surface impedance.

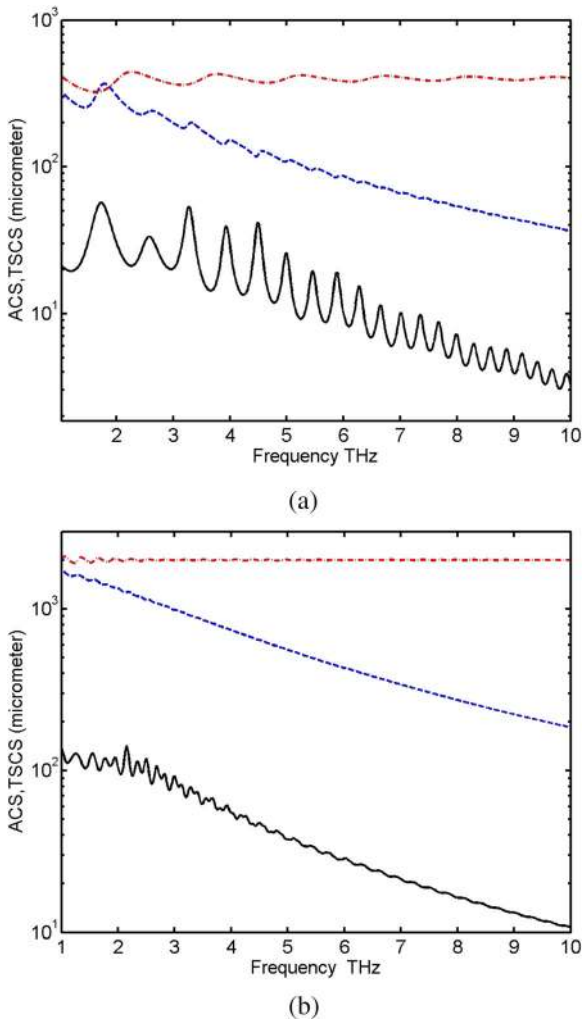

Fig. 2 H-case: Wave scattering and absorption by parabolic graphene reflectors versus the frequency in the THz range, for small-size reflector, $d = 200$ μm (**a**) and medium-size reflector, $d = 1000$ μm (**b**) Solid lines (*black*) and dashed lines (*blue*): ACS and TSCS for $\mu_c = 1$ eV. Dash-dotted lines (*red*): TSCS for the PEC reflector. The other parameters are the relative focal distance $f/d = 0.3$, the temperature $T = 300$ K, and the electron relaxation time $\tau = 1$ ps

The frequency scans of FA are plotted in Fig. 3 for the same two reflectors as in Fig. 2. It can be seen that the growth in μ_c increases FA at all frequencies. This happens because higher values of chemical potential μ_c lead to the lower values of the surface impedance of graphene that makes it less transparent. Then the curves get closer to the PEC case however still depart from it if the frequency becomes higher.

Periodic ripples on the plots of FA are explained by the free-space interference of the waves scattered by the edges of reflector: this explanation is becomes evident if one takes into account that their period is the same for the PEC and the graphene cases and is determined by reflector's size.

To obtain a fuller vision of the focusing ability of graphene reflector, we present a color map of this quantity as a function of two parameters: the focal ratio f/d and the frequency in the THz range – see Fig. 4. One can see that the optimal value of f/d, which provides maximum FA, is slightly below the value of 0.25 known to be optimal for PEC reflectors. New feature, as visible both from Figs. 3 and 4, is existence of an optimal frequency range where the focusing ability reaches maximum. This is apparently explained by the fact that, if the frequency grows, then the initial positive effect of increasing the electrical size of reflector becomes gradually overweighed by the negative effect of increasing the absolute value of graphene's impedance. Location and width of the optimal frequency band depends on the chemical potential, i.e. on graphene's doping.

Finally, in Fig. 5 we present the total near-field pattern for the graphene reflector with the aperture of $d = 450$ μm

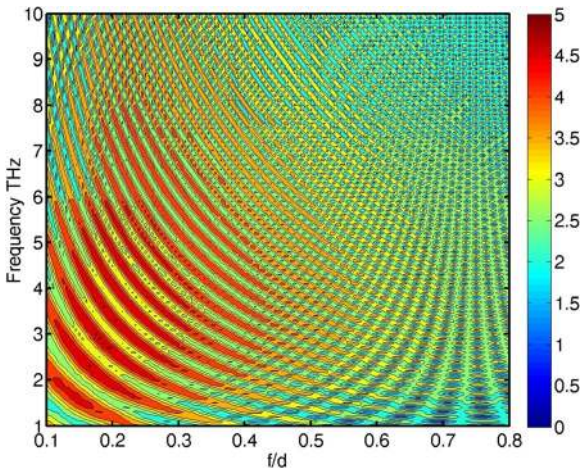

Fig. 4 H-case: Color map of the focusing ability as a function of f/d and frequency. Here, $d = 1000$ μm, $\mu_c = 1$ eV, $T = 300$ K, $\tau = 1$ ps

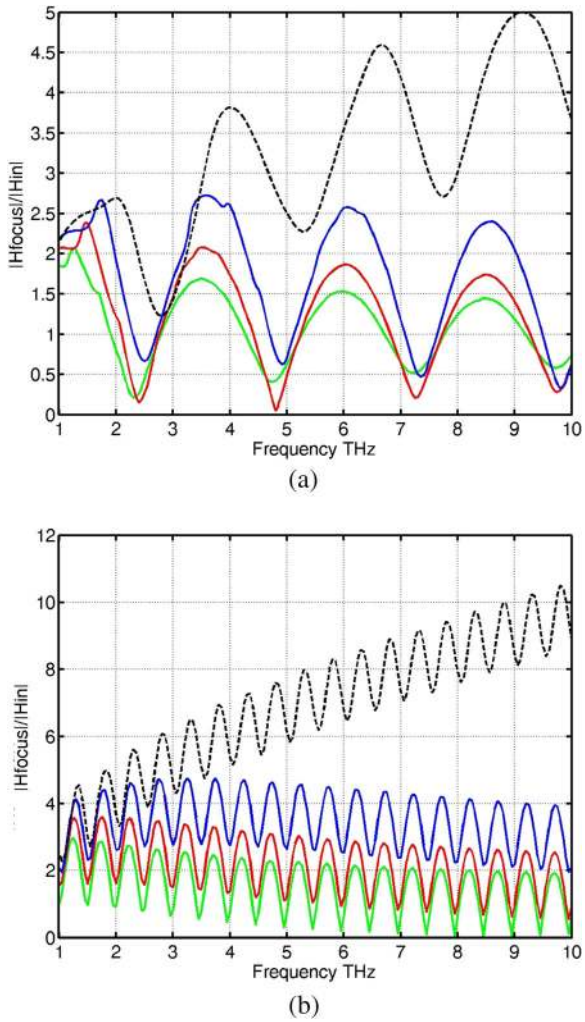

Fig. 3 H-case: Focusing ability of graphene reflectors versus the frequency in the THz range for small-size reflector, $d = 200$ μm (**a**) and medium-size reflector, $d = 1000$ μm (**b**) Solid line (*green*): $\mu_c = 0.3$ eV, solid line (*red*): $\mu_c = 0.5$ eV, solid line (*blue*): $\mu_c = 1$ eV. Dashed line (*black*): PEC reflector result. The other parameters are the same as in Fig. 2

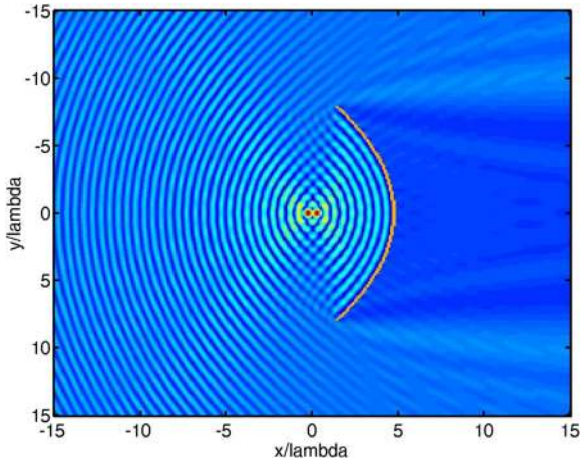

Fig. 5 H-case: Color map of the near-zone total field. Here, $f/d = 0.3$, $d = 450$ μm, $\mu_c = 1$ eV, $T = 300$ K, $\tau = 1$ ps and the frequency is 5 THz

(this is 7.5λ). Note the splitting of the focal domain to two bright spots along the axis of symmetry – this is a side effect, at the given frequency, of the finite size of reflector. Besides, one can see clearly observable interference of the waves scattered by the edges of the parabolic reflector in front of it and the presence of shadow behind it. Still this shadow is not very dark because the graphene reflector is partially transparent.

The further Figs. 6, 7, 8, and 9 present the numerical data analogous to in Figs. 2, 3, 4, and 5 however computed for the E-polarized wave incidence. Note the absence of the surface-plasmon resonances on the plots of ACS and FA as a function of frequency in Fig. 6a (compare to Fig. 2a) and Fig. 7a (compare to Fig. 3a), i.e. for a small-size reflector.

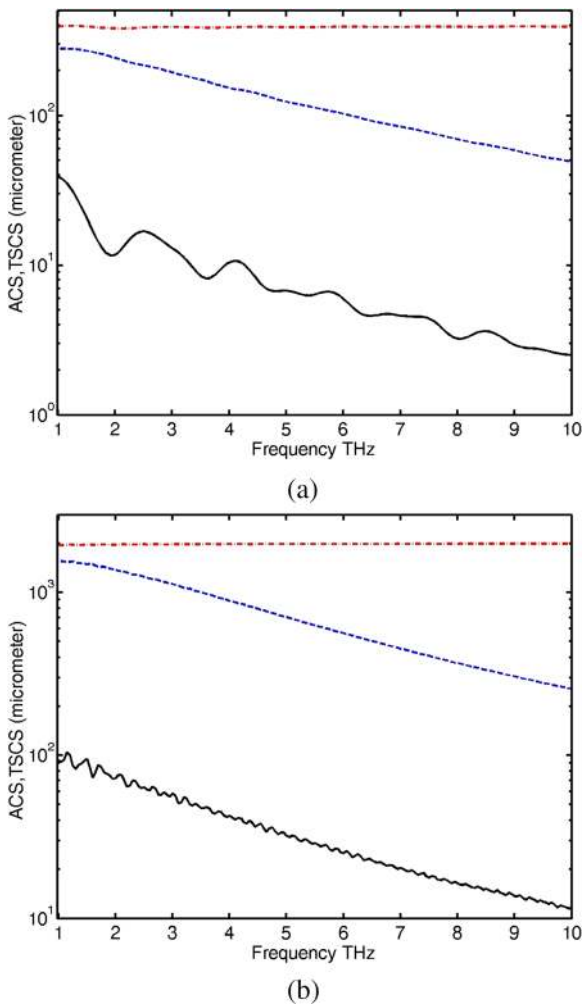

Fig. 6 E-case: Wave scattering and absorption by parabolic graphene reflectors versus the frequency in the THz range, for small-size reflector, $d = 200$ μm (**a**) and medium-size reflector, $d = 1000$ μm (**b**) Solid lines (*black*) and dashed lines (*blue*): ACS and TSCS for $\mu_c = 1$ eV. Dash-dotted lines (*red*): TSCS for the PEC reflector. The other parameters are $f/d = 0.3$, $T = 300$ K, $\tau = 1$ ps

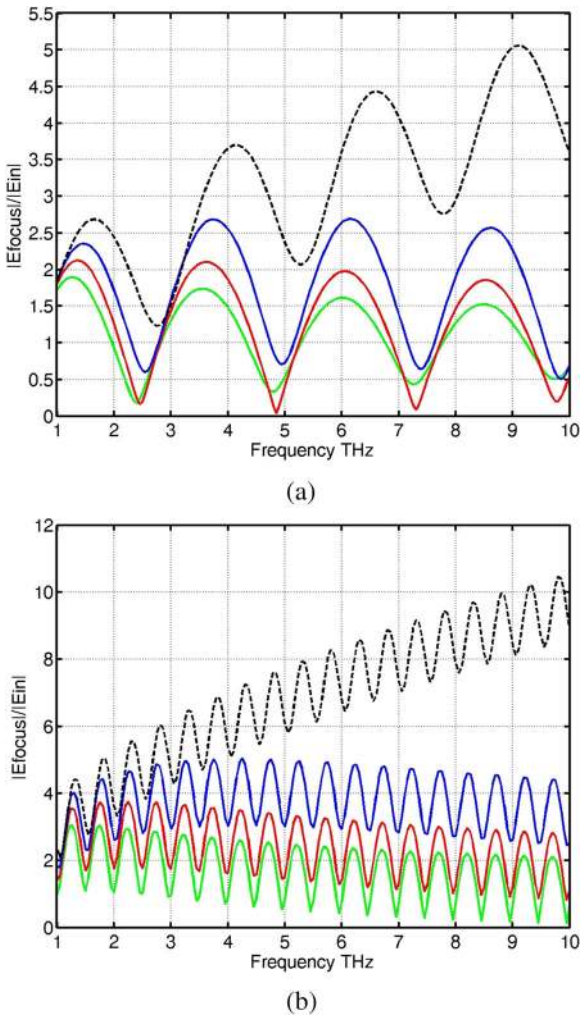

Fig. 7 E-case: Focusing ability of graphene reflectors versus the frequency in the THz range for small-size reflector, $d = 200$ μm (**a**) and medium-size reflector, $d = 1000$ μm (**b**) Solid line (*green*): $\mu_c = 0.3$ eV, solid line (*red*): $\mu_c = 0.5$ eV, solid line (*blue*): $\mu_c = 1$ eV. Dashed line (*black*): PEC result. The other parameters are the same as in Fig. 2

One can notice obvious similarities between plots and patterns for the H-case and the E-case if a graphene reflector is at least medium-size and the frequency is above 3 THz. This is apparently because the focusing of waves by a finite parabolic reflector, even a semi-transparent one, is essentially a high-frequency or quasi-optical effect. The main parameter in this case is just the electric size of reflector in terms of the free-space wavelength. The effect of the surface plasmon resonances is almost negligible at high frequencies, as well as dependence on the polarization in general. Note that in the E-polarization case the near-field portrait (Fig. 9) shows only one bright spot close to he geometrical focus of parabola.

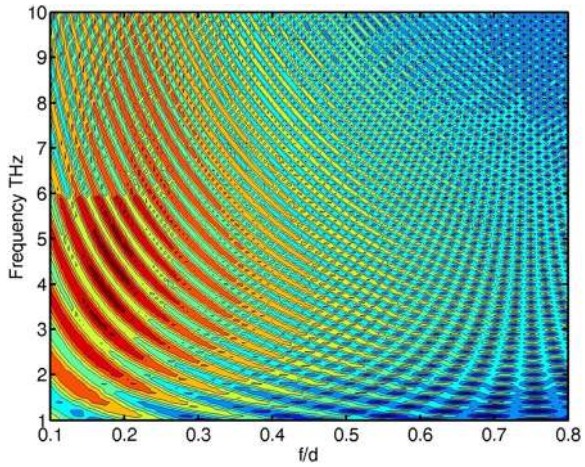

Fig. 8 E-case: Color map of the focusing ability as a function of *f/d* and frequency. Here, $d = 1000$ μm, $\mu_c = 1$ eV, $T = 300$ K, $\tau = 1$ ps

Conclusion

To summarize, a micro-size 2-D graphene reflector with parabolic profile, symmetrically illuminated by the H-polarized and E-polarized plane waves has been analyzed numerically using the MAR approach. The results show that the focusing ability of such a reflector is on par with a PEC reflector in the range of the frequency and the graphene parameters where the surface impedance of the latter is small. As follows from the Kubo formalism, this entails a necessity of working with higher values of chemical potential and electron relaxation time. This also means that for every fixed size of reflector there exists a band of optimal THz frequencies and the focusing ability is severely degraded at higher frequencies because of degradation of graphene's surface conductivity. The surface-plasmon resonances are present at lower THz frequencies in the H-wave case however their effect on the performance of micro-size graphene reflectors is small.

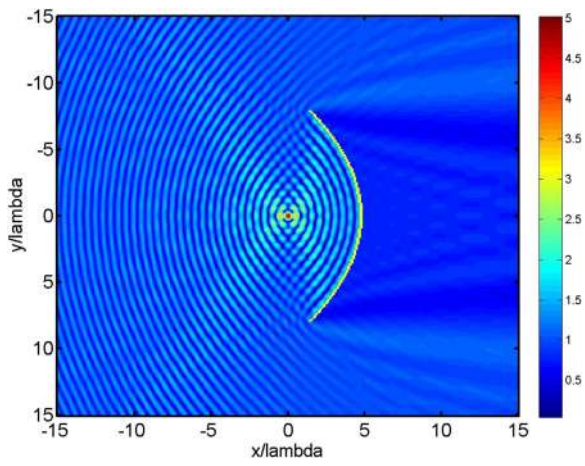

Fig. 9 E-case: Color map of the near-zone total field. Here, $f/d = 0.3$, $d = 450$ μm, $\mu_c = 1$ eV, $T = 300$ K, $\tau = 1$ ps and the frequency is 5 THz

Abbreviations

2-D: Two-dimensional; ACS: Absorption cross-section; BVP: Boundary-value problem; FA: Focusing ability; MAR: Method of analytical regularization; MoM: Method of moments; PEC: Perfect electric conductor; RHP: Riemann-Hilbet problem; SIE: Singular integral equation; SP: Surface plasmon; THz: Terahertz; TSCS: Total scattering cross-section

Funding

This work was not supported by any specific funding.

Authors' contributions

TO carried out the computations and drafted the manuscript. AA participated in the coordination of the study and in the interpretation of computed results. AN conceived of the study and finalized the manuscript. All authors read and approved the final manuscript.

Competing interests

The authors declare that they have no competing interests.

Publisher's Note

Author details

[1]Department Electrical and Electronics Engineering, Dokuz Eylul University, Buca, 35160 Izmir, Turkey. [2]Department Electrical and Electronics Engineering, Bilkent University, 06800 Ankara, Turkey. [3]Laboratory of Micro and Nano Optics, Institute of Radio-Physics and Electronics NASU, Kharkiv 61085, Ukraine.

Received: 30 January 2017 Accepted: 20 April 2017
Published online: 01 May 2017

References

1. Depine, R.A.: Graphene Optics: Electromagnetic Solution of Canonical Problems. IOP Concise Phys, Morgan and Claypool Publ, Bristol (2016)
2. Low, T., Avouris, P.: Graphene plasmonics for terahertz to mid-infrared applications. ACS Nano **8**, 1086–1101 (2014)
3. Rodrigo, D., Limaj, O., Janner, D., Etezadi, D., GarcíadeAbajo, F.J., Pruneri, V., Altug, H.: Mid-infrared plasmonic biosensing with graphene. Science **349**, 165–168 (2015)
4. Shapoval, O.V., Nosich, A.I.: Bulk refractive-index sensitivities of the THz-range plasmon resonances on a micro-size graphene strip. J Phys D Appl Phys **49**, 055105/8 (2016)
5. Du, X., Skachko, I., Barker, A., Andrei, E.Y.: Approaching ballistic transport in suspended graphene. Nat Immunol **3**, 491–495 (2008)
6. Orta, R., Savi, P., Tascone, R.: The effect of finite conductivity on frequency selective surface behavior. Electromagnetics **10**, 213–227 (1990)
7. Nosich, A.I., Okuno, Y., Shiraishi, T.: Scattering and absorption of E and H-polarized plane waves by a circularly curved resistive strip. Radio Sci **31**, 1733–1742 (1996)
8. Nosich, A.I.: Method of analytical regularization in computational photonics. Radio Sci **51**, 1421–1430 (2016)
9. Oğuzer, T., Altintas, A., Nosich, A.I.: Analysis of the elliptic profile cylindrical reflector with a non-uniform resistivity using the complex source and dual series approach: H-polarization case. Opt Quant Electron **45**, 797–812 (2013)
10. Zinenko, T.L.: Scattering and absorption of terahertz waves by a free-standing infinite grating of graphene strips: analytical regularization analysis. J Opt **17**, 055604/8 (2015)
11. Lucido, M.: A new high-efficient spectral-domain analysis of single and multiple coupled microstrip lines in planarly layered media. IEEE Trans Microw Theory Techn **60**, 2025–2034 (2012)
12. Oguzer, T., Altintas, A., Nosich, A.I.: Integral equation analysis of an arbitrary-profile and varying-resistivity cylindrical reflector illuminated by an E-polarized complex-source-point beam. J Opt Soc Am A **26**, 1525–1532 (2009)

13. Balaban, M.V., Shapoval, O.V., Nosich, A.I.: THz wave scattering by a graphene strip and a disk in the free space: integral equation analysis and surface plasmon resonances. J Opt **15**, 114007/9 (2013)
14. Shapoval, O.V., Gomez-Diaz, J.S., Perruisseau-Carrier, J., Mosig, J.R., Nosich, A.I.: Integral equation analysis of plane wave scattering by coplanar graphene-strip gratings in the THz range. IEEE Trans Terahertz Sci Technol **3**, 666–673 (2013)
15. Velichko, E.A.: Evaluation of a dielectric microtube with a graphene cover as a refractive-index sensor in the THz range,". J Opt **18**, 035008/11 (2016)
16. Oguzer, T., Altintas, A.: Focusing ability of a microsize graphene-based cylindrical reflector in the THz range illuminated by H-polarized electromagnetic plane wave. Proc Int Conf Math Methods Electromagn Theory (MMET-2016) **Lviv**, 232–235 (2016)